A large deformation finite element analysis solution for modelling dense sand

Solution d'analyse par éléments finis d'une large déformation pour la modélisation de sable dense

Li X.[1,2], Hu Y.[1], White D.[1]
[1] *University of Western Australian, Perth, Australia*
[2] *Beijing Jiaotong University, China*

ABSTRACT: To capture the softening behaviour of dense sand, an extended Mohr-Coulomb model was developed using a critical state framework. The model extends Bolton's correlations to capture dilatancy and peak strength, and is compatible with the remeshing and remapping strategies used in large deformation finite element analysis. This model is initially being used to simulate the behaviour of sand layers during foundation and spudcan penetration into uniform and stratified soils, but is applicable to a variety of problems that cannot be accurately simulated using conventional M-C plasticity alone.

RÉSUMÉ : Pour attraper le comportement s'adoucissant de sable, un modèle de Mohr-Coulomb étendu a été développé en utilisant un cadre critique d'état. Le modèle étend les corrélations de Bolton pour capturer la dilatance et la résistance de pic, et est compatible avec les stratégies de remaillage et remappage. Ce modèle est initialement utilisé pour simuler le comportement des couches de sable lors de la pénétration du caisson vers les sols feuilletés. Donc, il sera applicable à une variété de problèmes qui ne sont pas bien capturées en utilisant la plasticité M-C conventionnel.

KEYWORDS: Critical state; Large deformation analysis; Remeshing and mapping algorithm; Dilation; Shear band; Biaxial test.

1 INTRODUCTION

Sand can display dilation and strain-softening during shearing under certain stress and relative density conditions. There are numerous constitutive models developed to capture these characteristics (Manzari and Dafalias 1997; Li et al. 1999). However, to be able to implement such a constitutive model into finite element software for large deformation analysis, a relatively simple model is essential with the minimum of control variables involved. This is to ensure that the large deformation analysis can be kept stable.

Large deformation of sand has not been analysed widely since large deformation doesn't occur in general when a conventional foundation is placed on sand. However, when foundations – such as the spudcan foundations beneath offshore drilling rigs – are placed on sand overlying clay in offshore design, it is more likely for the sand layer to experience large deformation (Yu et al. 2010). Although large deformation of layered soils has been studied extensively for stiff clay over soft clay soils using large deformation FE analysis (LDFE) and centrifuge tests, fewer LDFE studies for sand over clay conditions have been executed since to date no suitable modelling approach exists for efficient simulation of the large strain behaviour of sand.

This paper describes an investigation into the dependency of bearing capacity on the large strain shearing characteristics of sand. An extended Mohr-Coulomb (MC) model was developed, which features strain-dependent hardening and softening using a critical state framework. The model uses state dependent dilatancy and friction angles. The controlling relations have been calibrated for a number of well-characterised sands, demonstrating that the model is a practical approach that can capture the specific responses of particular soils. The model was implemented in LDFE analysis (Hu and Randolph 1998a, 1998b) using the remeshing and interpolation technique with small strain model (RITSS).

The results of LDFE/RITSS with the extended MC model show that the volumetric and softening behaviour of sand has a significant influence on the penetration resistance of foundations during large penetration. When a shear band forms in sand, its dilatancy angle reaches zero and the sand finds the critical state. For foundations on uniform sand, this model shows how the variation in the bearing capacity factors N_q and N_γ is linked to density and initial stress state, as well as the fundamental strength property, the critical state friction angle.

The extended CSMC model coupled with LDFE shows great potential to capture sand behaviour through large deformations in a simple and efficient computational framework.

2 CRITICAL STATE MOHR-COULOMB (CSMC) MODEL

2.1 State dependent dilatancy angle and friction angle

Using the critical state concept, Been and Jefferies (1985) proposed a state parameter, Ψ to identify the current soil density state and to predict the subsequent shearing behaviour. The state parameter, Ψ is defined as:

$$\Psi = e - e_c \tag{1}$$

where e is the current void ratio; e_c is the critical state void ratio at current stress. The state parameter Ψ can be used to indicate the current volume change tendency of the sand and be linked to the dilation angle (Jefferies 1993; Manzari and Dafalias 1997; Li et al. 1999; Li 2002).

Been and Jefferies (1985) reported that both the peak friction angle ϕ_p and dilatancy angle ψ decrease with increasing Ψ. This idea also can be extended to loose sand where negative dilatancy (or contraction) occurs. A simple single parameter relation can be written as:

$$\tan\psi = -A\Psi \tag{2}$$

where A is a constant and is suggested as 1.2 (Li et al. 2013). The parameter A serves as a scale factor to the dilatancy angle, and it influences dilatancy angle in both the negative and positive regions of the state parameter Ψ, i.e. both dense and loose sands.

For a better fit to experimental data, a three-parameter relation can be written as:

$$\tan\psi \approx A(1-\exp^{sign(\Psi)m|\Psi|^n}) \tag{3}$$

where m, n are constants; n is a parameter controlling the curve shape; m is a parameter majorly influenced the curve shape with positive state parameter, i.e. loose sand.

Bolton (1986) linked peak friction and dilation angles by:

$$\phi_p \approx \phi_c + a\psi \tag{4}$$

where ϕ_c is critical friction angle; a is a constant. However, the value of a varies with soil stress condition and soil type (Li et al. 2003). Thus, the energy equation proposed by (Taylor 1948) is preferred here:

$$\tan\phi = \tan\phi_c + \tan\psi \tag{5}$$

Combining Eqs. 3 and 5, the relation between the mobilized friction angle and soil state parameter Ψ is illustrated in Fig. 1 with the variation of parameter A. The current state-dependent dilatancy angle and friction angle can be substituted into any modified Mohr-Coulomb (MC) model such as the hyperbolic MC model (Abbo and

Sloan 1995). This extension allows the MC model to capture soil hardening and softening behavior based on a critical state concept.

3 MODEL CALIBRATION

To implement state-dependent dilatancy and friction angles in the extended Mohr-Coulomb model developed here, the following parameters must be selected through the model calibration process (see Li et al. 2013 for further details):

(1) *Soil critical state line (CSL).* A power relation (Li and Wang 1998) can be more accurate than the conventional log-linear CSL for sand under a confining pressure no more than 2MPa:

$$e_c = e_\Gamma - \lambda(\frac{p'}{p_a})^\xi \quad (6)$$

where e_c is the critical void ratio at mean effective stress p'; e_Γ is the critical void ratio as mean effective stress diminishes to zero; p_a is a reference pressure taken as, p_a = 101 kPa (atmospheric pressure) for convenience; p' is the mean effective stress; λ is the slope of CSL in e versus $(p'/ p_a)^\xi$ plane, which is similar to the conventional compression index; ξ is a dimensionless constant. In this paper, λ is also termed as compression index and ξ is termed as compression power for convenience. For sand, ξ is typically 0.75 and the compression index can be estimated as $0.01C_u$ where C_u is the coefficient of uniformity of sand; e_Γ is estimated as $0.85\times e_{max}+0.15\times e_{min}$ where e_{max} and e_{min} are the maximum and minimum void ratios of the sand.

(2) *Dilatancy parameter A for Eq. 2 or dilatancy parameters A, m, n for Eq. 3.* For Eq. 2, A = 1.2 can be selected. For Eq. 3, m, n can be estimated as 3.5, 0.75 respectively. A is to be calibrated by experimental data and is typically in the range of 0.3 to 1.0.

(3) *Young's modulus E and Poisson's ratio ν.* The stiffness of sand varies with void ratio and stress state. Good predictions can be made using the following equation (Hardin and Richart 1963; Wang et al. 1990; Li et al. 1999; De and Basudhar 2008):

$$E = E_0 \frac{(2.97-e)^2}{1+e}\sqrt{\frac{p'}{p_a}} \quad (7)$$

where E_0 is suggested as 6~10 MPa (Carraro et al. 2009). The bulk and shear moduli, K and G can be calculated by the usual elastic relations from ν and E.

4 IMPLENTATION OF CSMC IN LDFE

4.1 LDFE with RITSS technique

Large deformation FE (LDFE) analysis is conducted by remeshing and interpolation technique with small strain (RITSS) (Hu & Randolph 1998a, b). This approach is coupled with a finite element package named AFENA (Carter & Balaam, 1995). To avoid large mesh distortion and achieve large deformation simulation, a series of small strain analysis increments (using AFENA) are combined with fully automatic remeshing of the entire domain, followed by interpolation of all field variables (such as stresses and material properties) from the old mesh to the new mesh.

During the mapping of field variables, some mapping error is inevitable. The fewer number of variables that must be carried to describe the current material state, the less error will be introduced after each mapping, thus the more accurate and convergent the large deformation analysis. When CSMC constitutive model is implemented to the LDFE/RITSS, void ratio e is the only extra variable required to be interpolated in addition to the stress field. Thus, numerical stability can be kept.

In the mesh generation/remeshing algorithm, the angle in one triangle element is limited in the range of 26~111°. Two criteria are used to trigger mesh refinement: (1) the distortion ratio ρ (which is the shortest distance from the mid node to a straight line joining the corner nodes, divided by the length of that straight line) exceeding 0.02; (2) the ratio between the maximum and minimum element edge lengths exceeding 100.

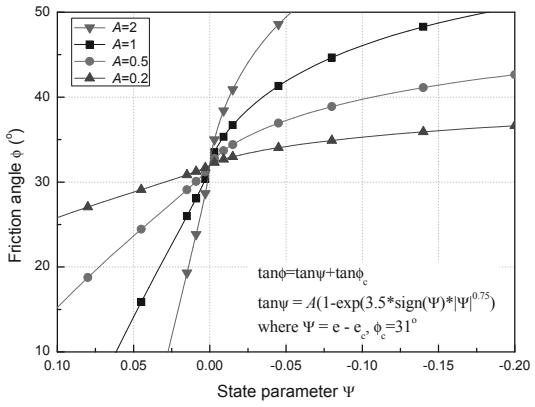

Fig. 1 Effect of parameter A on friction angle ϕ

4.2 Biaxial test

The calibration of the model parameters is illustrated using a single element simulation of a triaxial test and by a fully meshed simulation of a biaxial test, both in Ottowa sand (Alshibli et al. 2003). The close match of the prediction and the experimental data for a single element triaxial test provides the model parameters A = 0.36, m = 8, n = 0.75 (Fig. 2).

When the calibrated parameters were applied to the bi-axial element test conditions, a much lower peak is observed (Fig. 3). However, if the dilatancy angle is increased, as the parameter A in equation 2 is raised from 0.36 to 0.6, the CSMC model shows a similar peak as the experimental data (Fig. 3). Bolton (1986) has also suggested that the dilatancy angle in plane strain test is about 1.6 times of that in triaxial test. This shows that different parameters might be needed for triaxial and biaxial test conditions. In the biaxial test, the softening behaviour is captured very well.

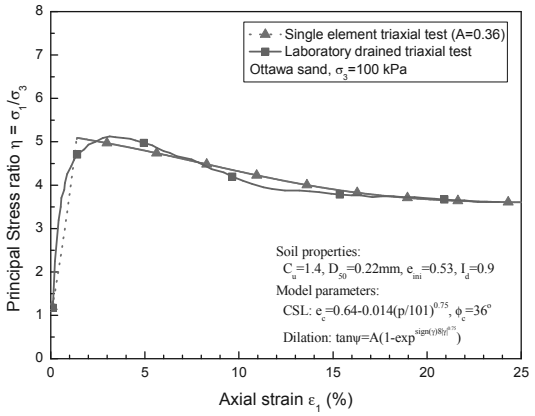

Fig. 2 Model calibration by single element triaxial test

Fig. 4 depicts the shear band formed in a biaxial test using the CSMC model. A single shear band is formed first at ~2% axial strain. Subsequently, a double shear band begins to form at ~3% axial strain and evolves gradually. This phenomenon is consistent with the observation in Alshibli et al. (2003).

The soil in the shear band yields and dilates gradually to the critical void ratio for this stress level, which is 0.61. The dilatancy angle decreases continuously until the soil reaches the critical state, mobilising ϕ_c. However, the soil outside the shear band remains at the initial void ratio, i.e. 0.54. The local strain in the shear band exceeds the external strain. The single element simulation (Fig. 2) shows a much slower decrease in the principal stress ratio after the peak than the biaxial test (Fig. 3). This confirms that the measured axial strain in laboratory tests that undergo localisation is only an apparent value (Fig. 4).

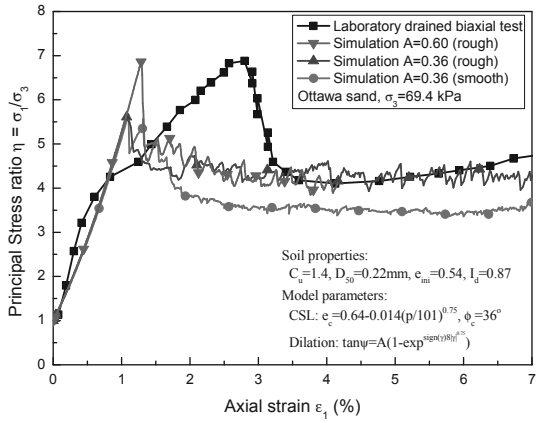

Fig. 3 Biaxial test result of Ottawa sand simulated by FEM

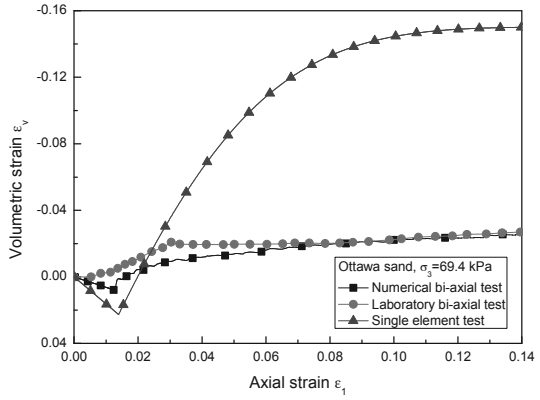

Fig. 4 ε_v-ε_1 relation in biaxial test

Strain localization is critical in explaining some laboratory test results where after the peak, the deviatoric stress, q, often decreases to a stable value much earlier for axial strain than volume strain (Samieh and Wong 1997; Salgado et al. 2000; Alshibli et al. 2003). In Alshibli et al. (2003), the stress starts to oscillate around a stable value after 10% axial strain, whilst the volume strain continuously increases even over 25% axial strain. Once a "central" shear band of soil at the critical state is formed, the apparent shear strength of whole sample reaches the critical value. However the volume of whole sample still increases with yielding of soil at the margins of the shear band (Fig. 5).

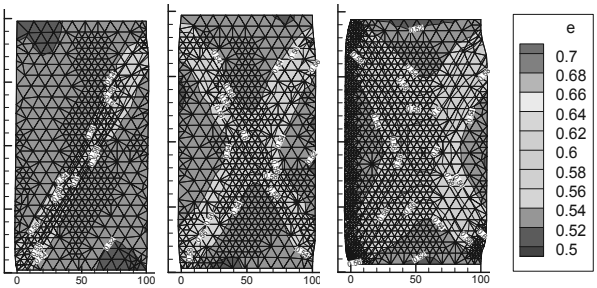

Fig. 5 Void ratio field: (a) ε_1=2%; (b) ε_1=3%; (c) ε_1=9%

The geometry of the specimen affects the shearing behavior. Biaxial simulation results with different sample aspect ratios are shown in Fig. 6. The σ_1-ε_1 relation is nearly identical in all three cases. However, the ε_v-ε_1 relation is dependent on the aspect ratio of the soil specimen and the shape of shear band formed.

5 BEARING CAPACITY OF A FOUNDATION ON SAND

The bearing capacity of circular plate on sand is analyzed by both limit analysis (using the ABC program, Martin 2004) and LDFE. In soil with self-weight the bearing capacity factor N_γ is often coupled with N_q although the two parts are not simply superposable. An N_q-N_γ bounding index ξ is defined as:

$$\xi = \frac{\gamma D}{q_{surf}} \tag{8}$$

where γD is a representative self-weight stress beneath the footing and q_{surf} is the surface surcharge. The coupled N_q and N_γ bearing capacity can be characterized by an integrated bearing capacity $N_{q\gamma}$ that varies with ξ and is defined as:

$$N_{q\gamma} = \frac{q_u}{q_{surf}} \tag{9}$$

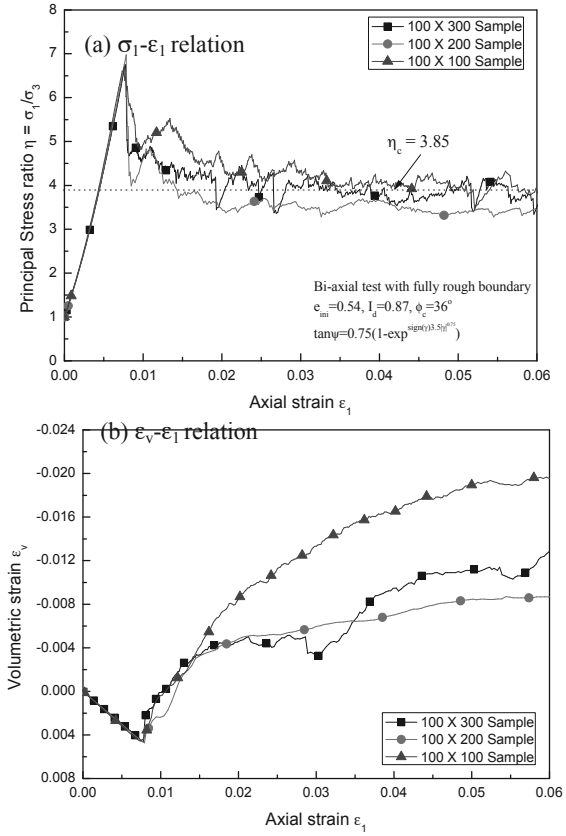

Fig. 6 Effect of sample geometry on biaxial shearing behaviour

Limit analysis using ABC shows that the integrated $N_{q\gamma}$ factor for a rough circular foundation can be approximated as (Fig. 7):

$$N_{q\gamma} = e^{2\pi \tan\phi}\left(1 + 0.48\tan\phi \frac{\xi}{1 + 0.0025\xi}\right) \tag{10}$$

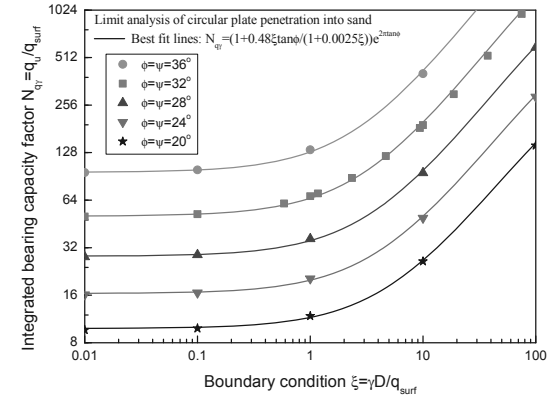

Fig. 7 Coupled bearing capacity factor $N_{q\gamma}$ for a circular foundation

Referring to Fig. 7, the integrated $N_{q\gamma}$ factor approaches a constant value with the decrease of the N_q-N_γ bounding index ξ. That ultimate value, $e^{2\pi\tan\phi}$, can be regarded as N_q. Similarly, the integrated $N_{q\gamma}$ of rough strip foundation can be calculated as,

$$N_{q\gamma} = \exp^{5\pi\tan\phi}(1+0.91\tan\phi\frac{\xi}{1+0.0025\xi}) \quad (11)$$

However, plasticity limit analysis involves certain assumptions: (1) an associated flow rule, i.e. $\psi = \phi$; (2) rigid plastic strength. The FEM method can consider the effect of soil stiffness and soil dilatancy angle on bearing capacity factor and the CSMC model allows the progressive changes in strength and stiffness during bearing failure to be captured.

Calculations of the N_q bearing capacity factor for a circular plate on weightless sand have been performed using LDFE and the MC model. The results show that both stiffness and dilatancy angle have a significant influence on the soil bearing capacity. The bearing capacity factor N_q varies by up to 50% for a realistic range of stiffness. The variation of N_q induced by the variation of dilatancy angle is no more than 15%. An empirical relation can be drawn for the estimation of N_q, as:

$$N_q = (0.6 - 0.06\ln\frac{q_{surf}}{E})e^{2\pi\tan\phi} \quad (12)$$

For the plate on weighted sand, the integrated $N_{q\gamma}$ is found to vary with soil stiffness, soil weight, soil dilatancy angle and soil dimension (as shown in Fig. 8). The FEM results (Fig. 9) show that the integrated $N_{q\gamma}$ approaches its ultimate value N_q if ξ is smaller than 2, as follows:

$$N_q = (\text{atan}\frac{0.015E}{\gamma D} + 0.3)(0.65+\sin\psi)\exp^{2\pi\tan\phi} \quad (13)$$

For all the cases, the integrated bearing capacity factor can be written as (seeing Fig. 8),

$$N_{qd} = \frac{0.45E}{q_{surf}}\frac{d}{D}e^{\tan\phi} \quad (14)$$

$$N_{qd} \le N_q(0.95+0.009(\frac{E}{\gamma D})^{0.5}\tan\phi\frac{\xi}{1+0.02\xi})$$

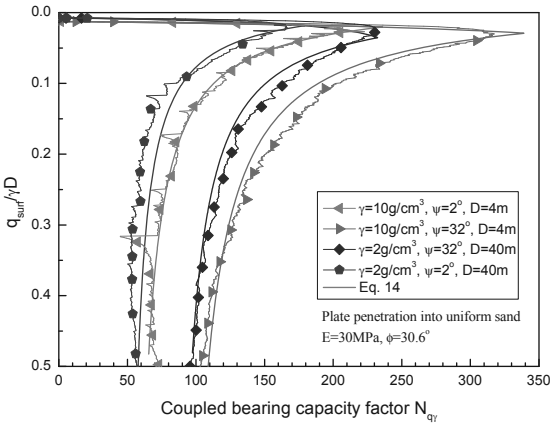

Fig. 8 Integrated bearing capacity factor $N_{q\gamma}$

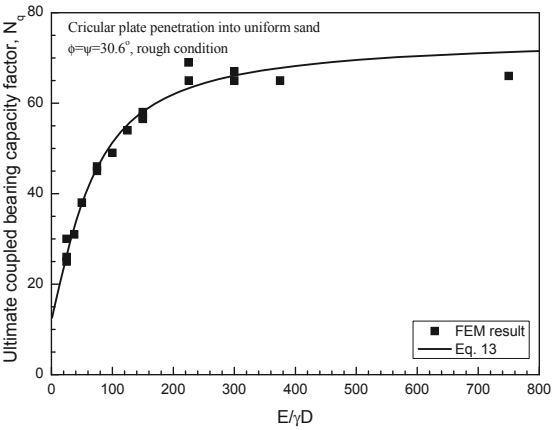

Fig. 9 Ultimate value of integrated bearing capacity factor N_q

6 CONCLUSION

In this paper, the classic Mohr-Coulomb (MC) model is extended to simulate soil hardening and softening behaviour based on critical state (CS) soil mechanics. Friction and dilation angles are linked with soil state parameter in an MC model. This new critical state Mohr-Coulomb (CSMC) model is verified by single element tests and large deformation finite element (LDFE) analysis using the RITSS method. The newly developed CSMC model can be easily applied to large deformation analysis and shows good stability.

ACKNOWLEDGEMENTS

This research is supported by The National Basic Research Program of China (973 Program, No. 2012CB026104) and the ARC Discovery Project DP1096764. The third author is supported by an ARC Future Fellowship and Shell.

REFERENCES

Abbo, A.J. and Sloan, S.W. 1995. A Smooth Hyperbolic Approximation to the Mohr-Coulomb Yield Criterion. Computers and Structures 54(3): 427-441.

Alshibli, K.A. Batiste, S.N. and Sture S. 2003. Strain localization in sand: plane strain versus triaxial compression. Journal of Geotechnical and Geoenvironmental Engineering, 129(6): 483-494.

Been, K. and Jefferies, M.G. 1985. A state parameter for sands. Géotechnique, 35(2): 99-112.

Been, K., Jefferies, M.G., and Hachey, J. 1991. The critical state of sands. Geotechnique, 41(3), 365–381.

Bolton, M.D. 1986. The strength and dilatancy of sands. Geotechnique, 36(1): 65-78.

Carter, J.P. and Balaam, N.P. 1995. AFENA users manual: Geotechnical Research Center, University of Sydney.

Hu, Y.X. and Randolph, M.F. 1998a. H-adaptive FE analysis of elasto-plastic non-homogeneous soil with large deformation. Computers and Geotechnics, 23(1-2): 61-83.

Hu, Y. & Randolph, M. F. 1998b. A practical numerical approach for large deformation problems in soil. *Int. J. Numerical and Analytical Meth. Geomech.* 22(5): 327-350.

Li X. Hu, Y.X. and White, D. 2013. Development of a critical state hyperbolic Mohr-Coulomb model for sand in large deformation FE analysis. Submitted to Geotechnique.

Li, X.S., Dafalias, Y.F., and Wang, Z.L. 1999. State-dependent dilatancy in critical-state constitutive modelling of sand. Candian Geotechnical Journal, 36(4): 599–611.

Ling, H.I. and Yang, S. 2006. A unified sand model based on critical state and generalized plasticity. J. of Eng. Mech., 132: 1380-1391.

Manzari, M.T., and Dafalias, Y.F. 1997. A critical state two-surface plasticity model for sands. Géotechnique, 47(2): 255–272.

Martin, C.M. 2004. ABC – Analysis of Bearing Capacity. http://www.eng.ox.ac.uk/civil/people/cmm/software.

Riemer, M.F. and Seed, R.B. 1997. Factors affecting apparent position of steady-state line. Journal of Geotechnical and Geoenviormental engineering, 123(3): 281-287.

Richard F., Wendell, H., Michael, M. and Gioacchino, V. Strain localization and undrained steady state of sand. Journal of Geotechnical and Geoenvironmental Engineering, 122(6): 462-473.

Samieh, A.M. and R.C.K. Wong. 1997. Deformation of Athabasca oil sand in triaxial compression tests at low effective stresses under varying boundary conditions. Canadian Geotech. J., 34: 985-990.

Taylor, D.W. 1948. Fundamentals of soil mechanics. Wiley. New York.

Verdugo, R., and Ishihara, K. 1996. The steady state of sandy soils. Soils Foundation, 36(2): 81-91.

Wang, Z.L., Dafalias, Y.F. and Shen, C.K. 1990. Bounding surface hypoplasticity model for sand. Journal of Engineering Mechanics, ASCE, 116(5): 983-1001.

Salgado R., Bandini, P. and Karim, A. 2000. Shear strength and stiffness of slity sand. Journal of Geotechnical and Geoenvironmental Engineering, 126: 451-461.

Yu, L., Hu, Y.X., Liu, J., Randolph, M. and Kong, X.J. 2012. Numerical study of spudcan penetration in loose sand overlying clay. Computers and Geotechnics, 46: 1-12

Carraro, H. Prezzi, M. and Salgado, R. 2009. Shear strength and Stiffness of sands containing Plastic or Nonplastic Fines. Journal of Geotech. and Geoenviromental Engineering, 135(9): 1167-1178.